Inorg. Chem. **2007**, *46*, 8784–8795

Anion–Solvent Dependence of Bistability in a Family of Meridional N-Donor-Ligand-Containing Iron(II) Spin Crossover Complexes

Ben A. Leita,[†] Suzanne M. Neville,[†] Gregory J. Halder,[‡] Boujemaa Moubaraki,[†] Cameron J. Kepert,[‡] Jean-François Létard,[§] and Keith S. Murray*[,†]

School of Chemistry, Building 23, Monash University, Clayton, Victoria 3800, Australia, School of Chemistry, University of Sydney, New South Wales 2006, Australia, and ICMCB, CNRS, Université Bordeaux 1, 87 avenue du Dr. A. Schweitzer, 33608 Pessac Cedex, France

Received June 3, 2007

Five mononuclear spin crossover iron(II) bis-meridional ligand complexes of the general formula $[Fe(L)_2](X)_2$·solvent, have been synthesized, where X = BF_4^- or ClO_4^-; L = 2-(1-pyridin-2-ylmethyl-1*H*-pyrazol-3-yl)-pyrazine (picpzpz) or 2-(3-(2-pyridyl)pyrazol-1-ylmethyl)pyridine) (picpypz); solvent = MeOH or EtOH. The magnetic and structural consequences of systematic variation of meridional ligand, solvent, and anion, including a desolvated species, have been investigated. The complex $[Fe(picpzpz)_2](BF_4)_2$·MeOH, **1·MeOH**, displays several unique properties including a two-step spin transition with a gradual higher-temperature step ($^1T_{1/2}$ = 197 K) and an abrupt low-temperature step with hysteresis ($^2T_{1/2}$ = 91/98 K) and a metastable intermediate spin state below 70 K with quench-cooling. Removal of the solvent methanol results in the loss of the abrupt step and associated hysteresis ($T_{1/2}$ = 150 K). The complexes $[Fe(picpzpz)_2](BF_4)_2$·EtOH (**1·EtOH**), $[Fe(picpzpz)_2](ClO_4)_2$·MeOH (**2·MeOH**), $[Fe(picpzpz)_2](ClO_4)_2$·EtOH (**2·EtOH**), and $[Fe(picpypz)_2](BF_4)_2$·MeOH (**3·MeOH**) all show gradual one-step spin transitions with $T_{1/2}$ values in the range 210–250 K. Photomagnetic LIESST measurements on **1·MeOH** reveal a near-quantitative excitation of high-spin sites and a unique two-step relaxation process related to the two-step thermal spin transition (^1T(LIESST) = 49 K and ^2T(LIESST) = 70 K). The structural consequences of the unusual spin transition displayed by **1·MeOH** have been investigated by single-crystal X-ray diffraction structural analyses between 25 and 293 K. Detailed characterization of the unit cell parameter evolution vs temperature reflects both the gradual high-temperature step and abrupt low-temperature step, including the thermal hysteresis, observed magnetically.

Introduction

Many examples exist of spin crossover (SCO) in iron(II) mononuclear systems and, more recently, dinuclear and polynuclear systems.[1] Within these examples a multitude of SCO features have been reported, including gradual and abrupt, one- and two-step, complete and incomplete transitions, and thermal hysteresis (or bistability).[1] Many of these features relate fundamentally to cooperative lattice effects, which, if strong, lead to abrupt SCO transitions (ideally at room temperature) with associated thermal hysteresis loops.[2] Such cooperative effects are commonly attributed to communication between SCO centers through electron−phonon interactions in the solid state but may also be augmented by first-order structural changes such as severe molecular rearrangement. This demonstrated ability of SCO compounds to exhibit bistability has led to their continued attention for applications in molecular switches and sensors and in devices such as displays and data storage media.[1,3] The achievement of bistability in SCO systems in a controlled and understandable manner is a nontrivial exercise, particularly in the case of mononuclear compounds, where a complex interplay of intermolecular interactions involving counterions, solvate

* To whom correspondence should be addressed. E-mail: keith.murray@sci.monash.edu.au. Tel: +61-3-99054512. Fax: +61-3-99054597.
† Monash University.
‡ University of Sydney.
§ Université Bordeaux.

(1) (a) Gütlich, P.; Garcia, Y.; Goodwin, H. A. *Chem. Soc. Rev.* **2000**, *29*, 419. (b) Létard, J.-F.; Guionneau, P.; Goux-Capes, L. *Top. Curr. Chem.* **2004**, *235*, 221. (c) Murray, K. S.; Kepert, C. J. *Top. Curr. Chem.* **2004**, *233*, 195.
(2) Gütlich, P.; Hauser, A.; Spiering, H. *Angew. Chem., Int. Ed. Engl.* **1994**, *33*, 2024.
(3) Kahn, O. *Nature* **1999**, *21*, 399.

10.1021/ic7010919 CCC: $37.00
Published on Web 09/14/2007

molecules, and ligand functionalities contribute to the presence or absence of an activation barrier in the transition.[1−4]

Within the large numbers of mononuclear iron(II) materials that exhibit SCO, a number of distinct families exist based on the metal ion coordination environment and/or the denticity of the ligand; such as mono-, bi-, tri-, and tetradentate ligands, fac and mer coordinations, and cis and trans coordinations.[1] This diversity allows us now to target specific chromophores to achieve SCO with relative confidence and to concentrate our attention, first, on carrying out detailed structural−magneto studies, and second, to use this information to enhance the degree of cooperativity in SCO systems.

The family of iron(II) materials that we target here are those containing bis-meridional ligands, for which numerous known examples encompass gradual and abrupt spin transitions, hysteresis, and thermal, pressure-, or light-induced SCO.[4−7] For example, the material $[Fe(dpzpy)_2]\cdot(BF_4)_2$ (dpzpy = 2,6-di(pyrazol-1-yl)pyridine) undergoes an abrupt spin transition at 261 K with a small hysteresis loop.[6a] Various other examples have been reported where the substituents of these meridional tris-imine-type ligands have been modified, including the addition of hydrogen-bonding functionality, and the magnetic consequences of these modifications followed.[6] Here, we present four iron(II) SCO complexes containing the asymmetric meridional ligand 2-(1-pyridin-2-ylmethyl-1H-pyrazol-3-yl)-pyrazine (picpzpz); this is the first reported example of this ligand and its iron(II) complexes. We report four analogues of the general formula $[Fe(picpzpz)_2](X)_2\cdot$solvent, where the solvent and anion are varied such that $X = BF_4^-$ or ClO_4^-, and solvent = MeOH or EtOH. Materials of this type have previously been shown to have anion dependence in their SCO character.[6] For comparative purposes, the complex $[Fe(picpypz)_2](BF_4)_2\cdot$MeOH has been prepared, which contains the meridional ligand 2-(3-(2-pyridyl)pyrazol-1-ylmethyl)pyridine) (picpypz). This ligand differs slightly to picpzpz through replacement of the pyrazine ring with pyridine. The perchlorate analogue of this material has been previously reported, $[Fe(picpypz)_2]\cdot(ClO_4)_2$, and was shown to undergo a gradual one-step full SCO with a $T_{1/2}$ value of ca. 175 K.[7] The X-ray structure of this complex was not reported, although those for its Co(II) and Ni(II) analogues were; in contrast to the materials presented here, these contain no included solvent.[7]

The consequences of SCO displayed in iron(II) complexes are most commonly followed directly via magnetic susceptibility studies or by following their Mössbauer spectral changes with temperature, pressure, and/or light irradiation.[1,5] In addition, crystallographic structural refinement is commonly used to follow the marked decrease in both the iron(II)−nitrogen bond lengths, by ca. 0.2 Å, and the unit cell volume, by typically ca. 10% depending on formula mass, over the transition from high-spin (HS) to low-spin (LS) states.[1] Such analyses have been used on occasion to follow spin transition curves through the collection of selected data points over narrow temperature ranges.[6,8−11] With the recent development of higher intensity X-ray sources, more sensitive CCD detectors, and faster processing times, improved capabilities have emerged for elucidating structural directing roles in the SCO phenomenon.[1,8] Recently, we have reported both dinuclear and polymeric materials that undergo two- and one-step spin transitions, respectively, where the detailed monitoring of the unit cell evolution was a key step in characterizing the SCO features.[11] We present here one of the most detailed examples of structural−magnetic correlation of anion−solvent-dependent thermal hysteresis, whereby the aforementioned hysteresis loop and thermal trapping at low temperature are observed both magnetically and through comprehensive crystallographic characterization of the temperature-dependent structure and unit cell evolution. The unit cell parameter analysis follows the entirety of the hysteretic two-step spin transition, using both heating and cooling modes, and closely mirrors the magnetic susceptibility data in displaying both hysteresis and thermal trapping at low temperatures.

Experimental Section

General. All reagents and solvents were of reagent grade and used as received. The ligand picpypz was made by a known method.[7] (***Caution:*** *iron(II) perchlorate was handled very carefully and in small amounts to avoid any potential explosions*). Microanalyses were performed by the Campbell Microanalytical Laboratory, Chemistry Department, University of Otago, Dunedin, New Zealand.

2-(1-(Pyridin-2-ylmethyl)-1*H*-pyrazol-3-yl)pyrazine (picpzpz). A mixture of 2-picolyl chloride hydrochloride (0.985 g, 6.0 mmol), 2-(1*H*-pyrazol-3-yl)-pyrazine (0.87 g, 6.0 mmol), toluene (75 mL), 40% aqueous NaOH (15 mL), and 40% aqueous tetra-*n*-butylammonium hydroxide (8 drops) was refluxed with stirring for 8 h and then stirred at room temperature overnight. The organic layer was then separated, dried over anhydrous Na_2SO_4, and filtered. Then the solvent was evaporated in vacuo to obtain a yellowish white solid. Recrystallization from acetone/hexane gave colorless needles of picpzpz. Yield 2.56 g (77%). mp = 101−103 °C. ESMS: $[M^+]$ 238 *m*/*z* and $[MNa^+]$ 260 *m*/*z*. Anal. Calcd (%) for $C_{13}H_{11}N_5$: C, 65.81; H, 4.67; N, 29.52. Found: C, 65.73; H, 4.56; N, 29.52. ^{1}H NMR $[(CD_3)_2SO$ (δ in ppm)] 9.00(d, 1H), 8.62(dd, 1H), 8.56−8.53(m, 2H), 8.02(d, 1H), 7.78(t, 1H), 7.34−7.30(m, 1H), 7.15(d, 1H), 6.95(d, 1H), 5.55 (s, 2H). ^{13}C NMR $[(CD_3)_2SO$ (δ in ppm)]

(4) Zhang, W.; Zhao, F.; Liu, T.; Wang, Z-M.; Gao, S. *Inorg. Chem.* **2007**, *46*, 2541.
(5) Gütlich, P.; Goodwin, H. A., *Top. Curr. Chem.* **2004**, *233*, 1.
(6) (a) Elhaïk, J.; Money, V. A.; Barrett, S. A.; Kilner, M. A.; Evans, I. R.; Halcrow, M. A. *Dalton Trans.* **2003**, 2053. (b) Money, V. A.; Elhaïk, J.; Evans, I. R.; Halcrow, M. A.; Howard, J. A. K. *Dalton Trans.* **2004**, 65. (c) Money, V. A.; Costa, J. S.; Marcén, S.; Chastanet, G.; Elhaïk, J.; Halcrow, M. A; Howard J. A. K.; Létard, J.-F. *Chem. Phys. Lett.* **2004**, *391*, 273. (d) Elhaïk, J.; Kilner, M. A.; Halcrow, M. A. *Dalton Trans.* **2006**, 823.
(7) Singh, S.; Mishra, V.; Mukherjee, J.; Seethalekshmi N.; Mukherjee, R. *Dalton Trans.* **2003**, 3392.
(8) Guionneau, P.; Marchivie, M.; Bravic, G.; Létard, J. −F.; Chasseau, D. *Top. Curr. Chem.* **2004**, *234*, 97.
(9) Galet, A.; Gaspar, A. B.; Muñoz, M. C.; Levchenko, G.; Real, J. A. *Inorg. Chem.* **2006**, 9670.
(10) Papanikolaou, D.; Margadonna, S.; Kosaka, W.; Ohkoshi, S.; Brunelli, M.; Prassides, K. *J. Am. Chem. Soc.* **2006**, *128*, 8358.
(11) (a) Neville, S. M.; Leita, B. A.; Offermann, D. A.; Duriska, M. B.; Moubaraki, B.; Chapman, K. W.; Halder, G. J.; Murray, K. S. *Eur. J. Inorg. Chem.* **2007**, 1073. (b) Amoore, J. J.; Kepert, C. J.; Cashion, J. D.; Moubaraki, B.; Neville, S. M.; Murray, K. S. *Chem. Eur. J.* **2006**, *12*, 8220.

156.3, 149.2, 148.8, 147.2, 144.1, 143.2, 141.0, 137.1, 133.2, 122.8, 121.6, 104.9, 56.9. IR (KBr disk, cm^{-1}), 3422br, 3111m, 2933m, 1939w, 1653w, 1587s, 1529m, 1491m, 1462m, 1434s, 1383m, 1360sh, 1325w, 1278m, 1236s, 1166sh, 1146s, 1112m, 1058s, 1015s, 958m, 851m, 781sh, 780s, 715m, 594m, 504m, 402s.

$[Fe(picpzpz)_2](BF_4)_2$·MeOH, 1·MeOH. To a solution of $Fe(BF_4)_2$·$6H_2O$ (68 mg, 0.2 mmol) in MeOH (5 mL) was added picpzpz (96 mg, 0.4 mmol) as a solid. This was stirred for 1 h and filtered, and then diffusion of ether overnight gave large red block crystals of $[Fe(picpzpz)_2](BF_4)_2$·MeOH. Yield 144 mg (98%). Anal. Calcd (%) for $C_{26}H_{22}N_{10}B_2F_8Fe$·MeOH: C, 44.06; H, 3.56; N, 19.03. Found: C, 43.98; H, 3.45; N, 18.93. IR (KBr disk, cm^{-1}): 3416br, 3128sh, 2928sh, 1775w, 1737w, 1702w, 1638sh, 1602m, 1526w, 1478w, 1437m, 1409s, 1356w, 1302w, 1246w, 1226w, 1061s, 1029s, 846w, 791w, 758m, 711w, 623w, 520w, 488w, 419w.

$[Fe(picpzpz)_2](BF_4)_2$·EtOH, 1·EtOH. Picpzpz (96 mg, 0.4 mmol) was added, as a solid, to a solution of $Fe(BF_4)_2$·$6H_2O$ (69 mg, 0.2 mmol) in EtOH (5 mL). The solution was stirred for 1 h, filtered, and after the diffusion of ether in to it overnight, a yellow/orange precipitate of $[Fe(picpzpz)_2](BF_4)_2$·EtOH was formed. Yield 130 mg (86%). Anal. Calcd (%) for $C_{26}H_{22}N_{10}B_2F_8Fe$·EtOH: C, 44.83; H, 3.76; N, 18.67. Found: C, 44.44; H, 3.43; N, 18.34. IR (KBr disk, cm^{-1}): 3426br, 1776w, 1733w, 1702w, 1636sh, 1610m, 1521w, 1468w, 1438m, 1412s, 1350w, 1302w, 1246w, 1226w, 1063s, 1029s, 843w, 794w, 752m, 711w, 633w, 521w, 485w.

$[Fe(picpzpz)_2](ClO_4)_2$·MeOH, 2·MeOH. To a solution of $Fe(ClO_4)_2$·$6H_2O$ (71 mg, 0.2 mmol) in MeOH (5 mL) was added picpzpz (96 mg, 0.4 mmol) as a solid. The solution was stirred for 1 h and filtered, and then diffusion of ether slowly yielded a yellow-orange precipitate of $[Fe(picpzpz)_2](ClO_4)_2$·MeOH. Crystals suitable for single-crystal X-ray analysis could not be obtained. Yield 109 mg (72%). Anal. Calcd (%) for $C_{26}H_{22}N_{10}Cl_2O_8Fe$·MeOH: C, 42.59; H, 3.44; N, 18.39. Found: C, 41.87; H, 3.21; N, 18.17. IR (KBr disk, cm^{-1}): 3422br, 3113sh, 1775w, 1720w, 1702w, 1638sh, 1602m, 1525w, 1479w, 1435sh, 1410s, 1355w, 1300w, 1246w, 1224w, 1151s, 1114sh, 1081s, 845w, 791w, 760m, 712w, 625s, 514w, 419w.

$[Fe(picpzpz)_2](ClO_4)_2$·EtOH, 2·EtOH. To a solution of $Fe(ClO_4)_2$·$6H_2O$ (71 mg, 0.2 mmol) in MeOH (5 mL) was added picpzpz (96 mg, 0.4 mmol) as a solid. After being stirred for 1 h, the solution was filtered, and then diffusion of ether yielded yellow-orange crystals of $[Fe(picpzpz)_2](ClO_4)_2$·EtOH. Yield 137 mg (98%). Anal. Calcd (%) for $C_{26}H_{22}N_{10}Cl_2O_8Fe$·EtOH: C,43.37; H, 3.64; N, 18.06. Found: C, 43.98; H, 3.47; N, 17.92. IR (KBr disk, cm^{-1}): 3443br, 1723w, 1710w, 1702w, 1648sh, 1526w, 1450w, 1435w, 1413s, 1351w, 1321m, 1246w, 1154s, 1113sh, 1084s, 847w, 792w, 763m, 715w, 631s, 513m.

$[Fe(picpypz)_2](BF_4)_2$·MeOH, 3·MeOH. 3·MeOH was prepared in a similar manner to **1·MeOH** but using the ligand picpypz. Yield of yellow-orange crystals 134 mg (91%). The crystals were unsuitable for single-crystal X-ray analysis. Anal. Calcd (%)for $C_{28}H_{24}N_8B_2F_8Fe$·MeOH: C, 47.45; H, 3.84; N, 15.26. Found: C, 47.11; H, 3.54; N, 14.97. IR (KBr disk, cm^{-1}): 3428br, 1767w, 1738w, 1712w, 1593s, 1474w, 1433m, 1413s, 1243w, 1224s, 1068s, 843w, 794w, 751m, 712m, 627w, 532w, 492w.

Magnetic Susceptibility Measurements. Magnetic susceptibility data were collected using a Quantum Design MPMS-5 SQUID magnetometer operating with an applied field of 1 T. The powdered samples were contained in a calibrated gelatine capsule held in the center of a drinking straw fixed to the end of the sample rod. In order to check for any crystallite orientation effects in the high-spin iron(II) forms ($^5T_{2g}$ ground states in octahedral symmetry), the samples were dispersed in Vaseline mulls and compared to the susceptibility data for the neat powders. Great care was exercised in ensuring that the solvated compounds such as **1·MeOH** did not lose any methanol during the measurements. Where indicated, samples were 'quench-cooled' by hand by direct introduction into the cavity at 4 K over a few seconds. The instrument was calibrated using a standard palladium sample of accurately known magnetization, supplied by Quantum Design, and also by the use of chemical calibrants such as $CuSO_4$·$5H_2O$ and $[Ni(en)_3](S_2O_3)$.

The photomagnetic measurements were performed using a Spectrum Physics Series 2025 Kr^+ laser ($\lambda = 532$ nm) coupled via an optical fiber to the cavity of a MPMS-55 Quantum Design SQUID magnetometer, and the power at the sample surface was adjusted to 5 mW cm^{-2}. It was noted that there was no change in the data due to irradiative heating of the sample. For the photomagnetic experiments, the samples consisted of a thin layer of compound, the weight of which was obtained by comparison of the thermal SCO curve with that of a more accurately weighed sample of the same compound. Our previously published, standardized method for determining LIESST properties was followed.[12] After being cooled slowly to 10 K, the sample, now in the low-spin state, was irradiated and the change in magnetism followed. When the saturation point had been reached, the irradiation was ceased and the temperature increased at a rate of 0.3 K min^{-1} while the magnetization was measured every 1 K. T(LIESST) was determined from the minimum of the $\partial\chi_M T/\partial T$ vs T curve.

Optical Reflectivity. The measurement of the diffuse absorption spectra and reflectivity signal were performed using a custom-built setup equipped with a SM240 spectrometer (Opton Laser International). This equipment allows the diffuse absorption spectra, within the range of 500−900 nm at a given temperature, and the temperature dependence (5−290 K) of the reflectivity signal at a selected wavelength (±2.5 nm) to be recorded. The diffuse reflectance spectrum was calibrated with respect to charcoal activated (Merck) as black standard and barium sulfate ($BaSO_4$, Din 5033, Merck) as white standard. This analysis was performed directly on a thin layer of the available solid samples in the form of polycrystalline powders; no dispersion in a matrix was required.

Crystallographic Data Collection and Refinement Diffraction Data for 1·MeOH. 25 (slow cooled, 25s), 25 (quench cooled, 25q), 123 and 293 K were collected on a Bruker SMART 1000 CCD diffractometer using graphite-monochromated Mo Kα ($\lambda = 0.71073$ Å) radiation and Oxford Cryosystems 600 series (nitrogen) or HeliX (helium gas) cryostreams. The temperature dependence of the unit cell parameters was also monitored using single-crystal X-ray diffraction. Short sets of diffraction data suitable for accurate determination of the unit cell parameters (three sets of 20 0.3° frames)[13] were collected as the temperature was ramped according to the two following measurement profiles.

Measurement One: Helium Gas Cryostream 25−115 K. The crystal was mounted in a thin film of perfluoropolyether oil on a mohair fiber and quench-cooled to 25 K in order to trap the compound in the HS/LS state. A full structural determination was completed at this temperature (labeled 25q). The evolution of the unit cell parameter was subsequently followed with heating to 80 K at 20 K h^{-1}. Between 80 and 115 K, with both heating and cooling, the temperature was stepped at 5 K intervals between unit cell determinations to carefully elucidate the hysteretic nature of the abrupt LS to HS/LS transition. The crystal was then cooled from 80 to 25 K at 20 K h^{-1} while continually determining unit

(12) Létard, J.-F. *J. Mater. Chem.* **2006**, *16*, 2550.
(13) *SMART, SAINT, and XPREP: Area Detector control and data integration and reduction software*; Bruker Analytical X-ray Instruments Inc.: Madison, WI, 1995.

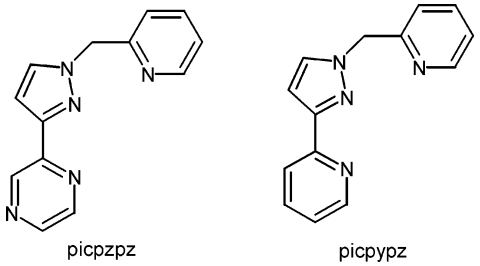

Figure 1. N-Donor meridional tridentate ligands 2-(1-pyridin-2-ylmethyl-1*H*-pyrazol-3-yl)-pyrazine (picpzpz) and 2-(3-(2-pyridyl)pyrazol-1-ylmethyl)pyridine) (picpypz).

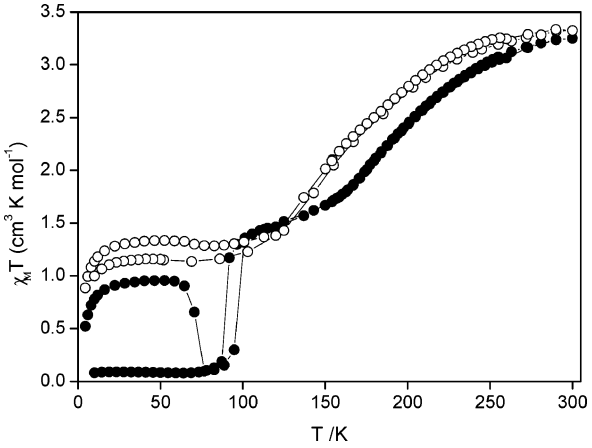

Figure 2. Plot of $\chi_M T$ vs T for $[Fe(picpzpz)_2](BF_4)_2$·MeOH, **1·MeOH** (●), when cooled slowly from 300 K and then warmed slowly, and for the desolvated species **1** (○) under slow cooling and slow warming. Thermal trapping of ∼30% HS fraction can be seen for **1·MeOH** between 2 and 60 K when the sample is quench-cooled to 2 K, then warmed (●)

cell parameters, where a full structural determination of the compound in the fully LS state was completed (labeled 25s).

Measurement Two: Nitrogen Gas Cryostream 105−293 K. A second crystal was mounted with a thin smear of grease in an open-ended glass capillary and quench-cooled to 105 K. Multiple unit cell data were collected between 105 and 115 K to confirm consistency with Measurement One. A full structural determination of the compound in the HS/LS state was completed at 123 K (labeled 123). Continuous variable-temperature measurements of the unit cell parameters were performed with heating to 293 K at 20 K h^{-1}, where a final full structural determination was completed for the compound in the HS state (labeled 293). We note that use of separate crystals resulted in a slight mismatch between data from Measurements One and Two (Figure 9).

Single-crystal data for **2·EtOH** were collected on a Nonius Kappa CCD diffractometer using graphite-monochromated Mo Kα ($\lambda = 0.71073$ Å) radiation and an Oxford Cryosystems 600 series (nitrogen) cryostream.

Empirical absorption corrections were applied to all data using SADABS.[14] The structures were solved with SHELXS-97[15] and refined with SHELXL-97[16] from data reduced with SAINT+ V.6.02.[13] All non-hydrogen atoms were modeled anisotropically except those of the methanol molecules and the disordered fluorine

(14) Sheldrick, G. M. *SADABS: Empirical absorption correction program for area detector data*; University of Göttingen: Göttingen, Germany, 1996.
(15) Sheldrick, G. M. *SHELXS-97: Program for crystal structure solution*; University of Göttingen: Göttingen, Germany, 1997.
(16) Sheldrick, G. M. *SHELXCIF-97: Program for generation of crystallographic tables*; University of Göttingen: Göttingen, Germany, 1997.

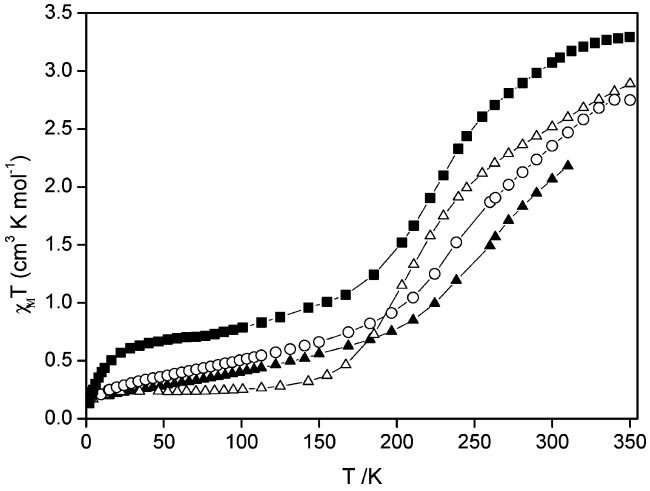

Figure 3. Plot of $\chi_M T$ vs T for **2·MeOH** (■), **1·EtOH** (○), **2·EtOH** (▲), and **3·MeOH** (△).

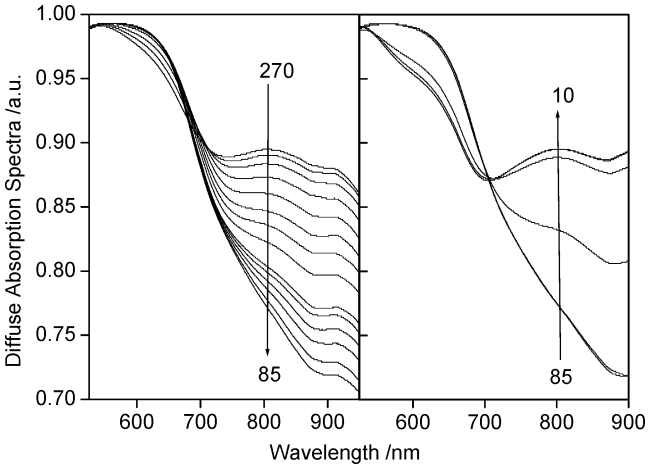

Figure 4. Plot of the diffuse absorption spectra of **1·MeOH** vs wavelength over the temperature range 85−270 K (left) for the normal spin transition and the range 85−10 K for the photoinduced effect.

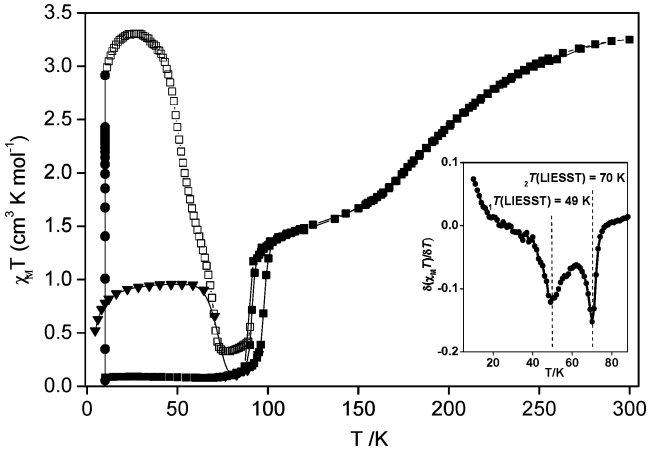

Figure 5. Plot of $\chi_M T$ vs T over the range 10−275 K for the photomagnetic effect for **1·MeOH** (irradiation 512 nm (●) followed by relaxation (□) and thermal spin transition (■)). For comparative purposes, the thermal trapping between 2 and 60 K upon quench cooling is shown (▼) Inset: Plot of $\delta\chi_M T/\delta T$ vs T indicating a T(LIESST) values of 49 and 70 K at the two minima.

atoms in the **1·MeOH** 123 and 293 K structures. CCDC-645187-91 contains the crystal data for this paper. These data can be obtained free of charge via www.ccdc.cam.ac.uk/conts/retrieving-

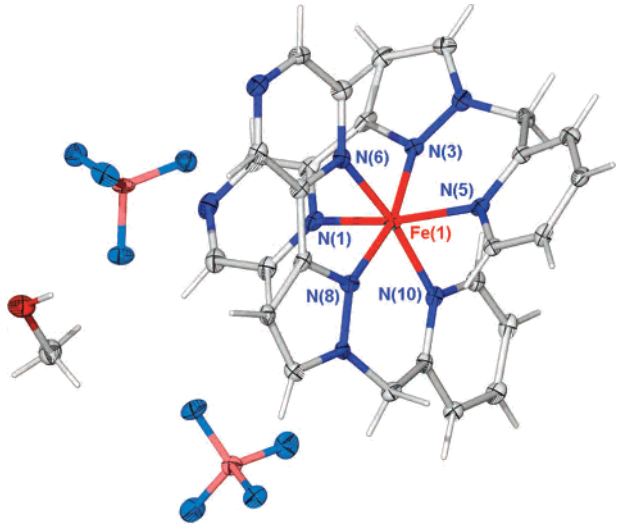

Figure 6. ORTEP representation of the crystal structure and atom labeling scheme of **1·MeOH** at 25 K (25s) where there is no disorder in either the solvent or anion.

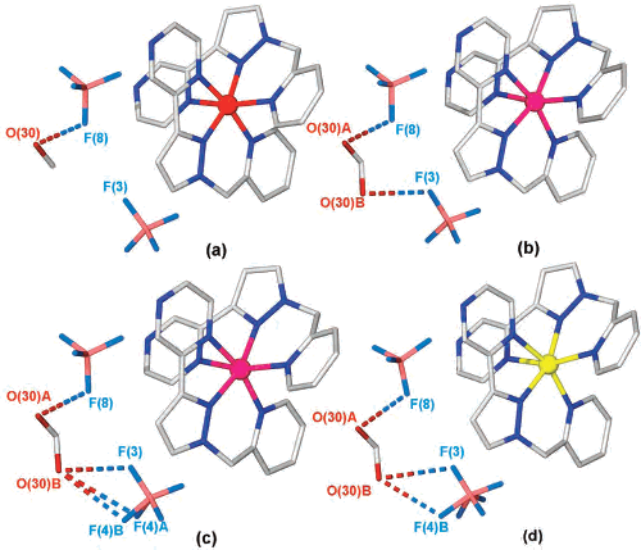

Figure 7. Stick representation of the hydrogen-bonding interactions between the solvent methanol and BF_4^- anion in **1·MeOH**. (a) 25 K slow-cooled (25 s), (b) 25 K quench-cooled (25 q), (c) 123 K, and (d) 298 K. The methanol molecule is disordered in (b), (c), and (d), and the BF_4^- anion is disordered in (c) and (d). Hydrogen atoms have been omitted for clarity. Iron(II) ions are represented as spheres in a color highlighting their respective spin states (HS, yellow; HS/LS, pink; LS, red).

.html (or from the Cambridge Crystallographic Data Centre, 12 Union Road, Cambridge, CB21EZ, UK; fax: (+44)1223-336-033; or deposit@ccdc.cam.ac.uk).

Results

Synthesis. The ligand picpzpz (Figure 1) was prepared using a slight modification to a method reported by Singh et al.[7] for picpypz. The iron(II) chelates were made in methanol by adding ligand to metal salt, in a 2:1 ratio. Ether diffusion yielded red crystals for **1·MeOH** and a yellow-orange powder for **2·MeOH** in almost quantitative yields. The complexes were characterized by single-crystal X-ray diffraction, IR spectra, and microanalyses. Coordinated picpzpz IR bands characteristically occurred at 1526, 1410, and 1246 cm^{-1}.

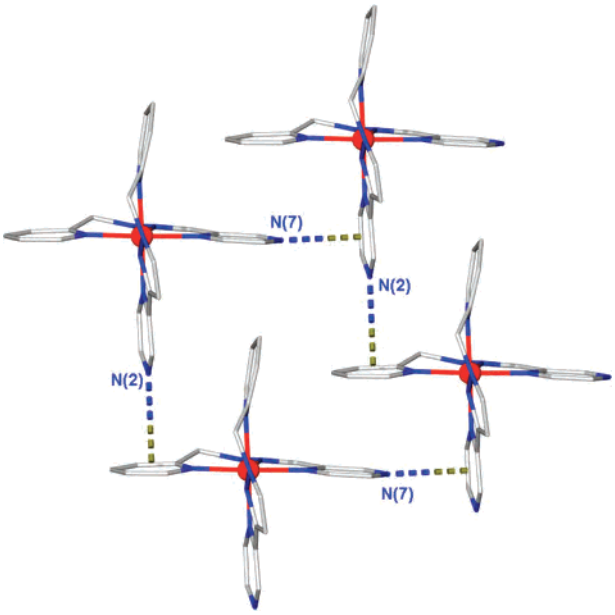

Figure 8. Stick representation of the intermolecular contacts in the *ab* plane for **1·MeOH** of the type N(lone pair)···centroid of neighboring pyrazine π-system. Hydrogen atoms have been omitted, and iron(II) ions are represented as spheres.

Magnetic Susceptibility and Photomagnetic Effect. [Fe(picpzpz)$_2$](BF$_4$)$_2$·MeOH (1·MeOH). The $\chi_M T$ vs T data for **1·MeOH** are shown in Figure 2. A two-step spin transition, reproducible from sample to sample, was observed. The $\chi_M T$ values remained approximately constant at 3.261 $cm^3\ mol^{-1}$ K when the sample was in the HS state. As the sample was cooled slowly, it underwent a gradual half SCO between 300 and 130 K, where the $\chi_M T$ values reached a plateau value of 1.395 $cm^3\ mol^{-1}$ K between 105 and 125 K. The $T_{1/2}$ of the broad spin transition is ca. 197 K (labeled $^1T_{1/2}$). In the plateau region, the complex is in a 50% HS to 50% LS state. The $\chi_M T$ values then underwent a very sharp decrease to ca. 0.128 $cm^3\ mol^{-1}$ K, with $^2T_{1/2}$ of 85 K. The complex is now in its fully LS form and the $\chi_M T$ values remained constant at 0.095 $cm^3\ mol^{-1}$ K between 75 and 4 K. When the complex was warmed, a hysteresis loop of 7 K width was observed at $^2T_{1/2} = 91$ and 98 K. This increase in $\chi_M T$ was equally sharp as it was on cooling. With continued warming, the $\chi_M T$ values followed those of the initial cooling cycle, such that there was no thermal hysteresis in the gradual spin change that occurred between 300 and 130 K.

The sample of **1·MeOH** was quench-cooled to 4 K. With heating to ca. 10 K, a small increase in $\chi_M T$ was observed due to the zero-field splitting of the $^5B_2$ ground state (assumed compressed tetragonal symmetry) of the trapped HS Fe(II) form. At 10 K, a plateau at 0.964 $cm^3\ mol^{-1}$ K was observed which remained with heating until 65 K (Figure 2). When the temperature was further increased, the $\chi_M T$ values decreased and reached the LS value, again, at ca. 80 K. This metastable HS state is accessible for **1·MeOH** upon quench-cooling, and this is an indication that we can reach such a state via irradiation (LIESST effect). A comparison of the $\chi_M T$ values reached at the plateau (0.964 $cm^3\ mol^{-1}$ K), and the response recorded at room temperature for a purely HS state indicates that ~30% of HS fraction had been

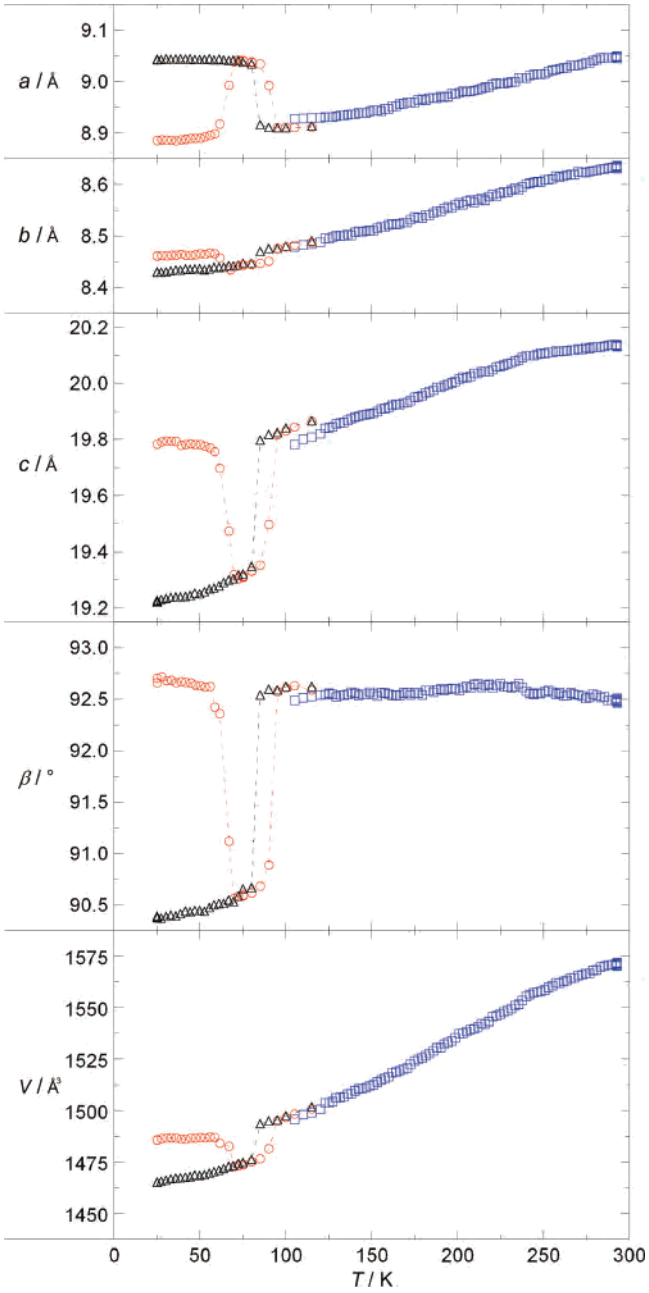

Figure 9. Changes in unit cell parameter vs temperature (K) for a crystal of **1·MeOH**. Quench-cooled data (red) over the range 25−115 K, slow-cooled data (black) over the range 25−115 K, and heating 105−293 K (blue).

thermally trapped. The non-quantitative trapping of a quench cooled state is not surprising, as the quench-cooling experiment was conducted over a few seconds, thus allowing some relaxation. The *T*(TIESST) value, i.e., the limiting temperature of thermally induced excited spin state trapping by analogy with the light-induced *T*(LIESST) measurement, is 70 K.

Magnetic susceptibility measurements on the desolvated sample, **1**, are shown in Figure 2. At room temperature, the complex was fully HS with a $\chi_M T$ value of 3.329 $cm^3\ mol^{-1}$ K, similar to that found for **1·MeOH**. Upon slow cooling of **1**, a gradual, incomplete crossover was observed between 300 and 120 K, and then the $\chi_M T$ values plateaued at 1.167 $cm^3\ mol^{-1}$ K between 120 and 10 K, with $T_{1/2}$ of ca. 150 K. As the sample was warmed, a slightly lower path was followed up to 100 K until, thereafter, the $\chi_M T$ values returned to those observed upon cooling.

1·EtOH, 2·MeOH, and 2·EtOH. The magnetic features of picpzpz-containing compounds with different anion or solvates to those in **1·MeOH** were explored, showing that the SCO properties of these complexes are both solvent and anion dependent (Figure 3).

The complex **1·EtOH** displayed a gradual, incomplete SCO, the incompleteness probably due to some small impurities/surface effects. (Figure 3). The $\chi_M T$ value underwent a very gradual decrease upon cooling, from 2.76 $cm^3\ mol^{-1}$ K at 300 K, to reach a minimum of 0.162 $cm^3\ mol^{-1}$ K at 4 K. The $T_{1/2}$ temperature is ca. 235 K. No thermal hysteresis or thermal trapping due to rapid cooling was observed for this compound.

The complex **2·MeOH** which remains structurally uncharacterized due to its poor crystallinity, displays a gradual, incomplete SCO (Figure 3). The $\chi_M T$ value underwent a very gradual decrease from 3.31 $cm^3\ moln^{-1}$ K at 300 K to reach a plateau of 0.703 $cm^3\ mol^{-1}$ K between 100 and 20 K. The $T_{1/2}$ temperature is ca. 230 K. In this plateau temperature range, there are ∼40% HS centers present. No thermal hysteresis or thermal trapping due to rapid cooling was observed for this compound.

The compound **2·EtOH** displays a very gradual spin transition, with a temperature dependence similar to that observed for the BF_4^- analogue, **1·EtOH**, and a $T_{1/2}$ value of ca. 250 K (Figure 3). The $\chi_M T$ value at 123 K of *ca.* 0.5 $cm^3\ mol^{-1}$ K is a little higher than might be expected given that the Fe−N bond lengths at this temperature are consistent with a fully LS state (Table 2).

3·MeOH. The compound **3·MeOH** displays a single, gradual SCO from a $\chi_M T$ value of 2.88 $cm^3\ mol^{-1}$ K at 300 K to a plateau of 0.246 $cm^3\ mol^{-1}$ K below 125 K. The $T_{1/2}$ is ca. 210 K (Figure 3). The LS plateau has $\chi_M T$ values rather higher than normal, even allowing for second-order Zeeman effects in the LS $^1A_{1g}$ state, and these most probably arise from some HS sites remaining and being responsible for the more rapid decrease in $\chi_M T$ values below 10 K. No thermal hysteresis was observed. The closely related complex, $[Fe(picpypz)_2](ClO_4)_2$, has previously been reported and undergoes a gradual one-step SCO with $\chi_M T$ values of 3.36 and 0.59 $cm^3\ mol^{-1}$ K at 300 and 70 K, respectively, with a $T_{1/2}$ of ca. 175 K.[7]

LIESST Studies on 1·MeOH. Thermal SCO can be monitored conveniently through following the visible spectrum of the solid sample as a function of temperature, as measured at the surface of the sample by diffuse reflectance.[17] Figure 4 shows the spectral changes for compound **1·MeOH** measured along its thermal spin transition. The band at 800−850 nm corresponds to a d−d transition of the HS iron(II) center, while the absorptions around 500−650 nm can be

(17) Desaix, A.; Roubeau, O.; Jeftic, J.; Haasnoot, J. G.; Boukheddaden, K.; Codjovi, E.; Linares, J.; Nogues, M.; Varret, F. *Eur. Phys. J. B* **1998**, *6*, 183.

Table 1. Crystallographic Data for **1·MeOH** at 25 K Slowly-Cooled (25s), 25 K Quench-Cooled (25q), 123 K, and 293 K and **2·EtOH** at 123 K

compound	**1·MeOH**				**2·EtOH**
label	25s	25q	123	293	123
spin state	LS	LS/HS	LS/HS	HS	LS
formula	$C_{27}H_{26}B_2F_8FeN_{10}O$	$C_{27}H_{26}B_2F_8FeN_{10}O$	$C_{27}H_{26}B_2F_8FeN_{10}O$	$C_{27}H_{26}B_2F_8FeN_{10}O$	$C_{28}H_{28}Cl_2FeN_{10}O_9$
formula mass/ g mol^{-1}	736.05	736.05	736.05	736.05	775.35
temp/K	25(2)	25(2)	123 (2)	293 (2)	123(2)
crystal system	monoclinic	monoclinic	monoclinic	monoclinic	monoclinic
space group	*Pn*	*Pn*	*Pn*	*Pn*	$P2_1/n$
Z	2	2	2	2	4
a/Å	9.048(7)	8.891(9)	8.9178(5)	9.0305(6)	8.7144(17)
b/Å	8.427(7)	8.463(9)	8.4858(4)	8.6282(6)	39.851(8)
c/Å	19.222(16)	19.75(2)	19.8148(10)	20.1137(13)	9.1308(18)
α/°	90	90	90	90	90
β/°	90.213(13)	92.588(16)	92.5160(10)	92.4540(10)	93.99(3)
γ/°	90	90	90	90	90
V/Å^3	1466(2)	1485(3)	1498.03(13)	1565.76(18)	3163.2(11)
D_c/g cm^{-1}	1.668	1.646	1.632	1.561	1.628
μ(Mo Kα)/cm^{-1}	0.610	0.602	0.597	0.571	0.717
data/restraints/ params	4956/2/444	5832/3/450	6785/3/449	6274/3/443	6807/0/452
Flack param	0.037(13)	0.055(10)	0.004(12)	0.012(18)	−
$R(F)$ [$I > 2\sigma(I)$, all]	0.0352, 0.0381	0.0292, 0.0322	0.0363, 0.0446	0.0468, 0.0646	0.0640, 0.1164
$R_w(F^2)$ [$I > 2\sigma(I)$]	0.0891, 0.0908	0.0701, 0.0715	0.0818, 0.0875	0.1115, 0.1260	0.1600, 0.1858
GOF	1.042	1.012	1.064	1.064	1.019

reasonably assigned to both d−d and MLCT transitions of the LS material.[21] The drastic decrease in intensity of the 800−850 nm absorption band over the range 270−85 K (Figure 4) reflects the thermal spin transition occurring at ca. 200 K, i.e., a decrease of the d−d band along the HS to LS transition. Furthermore, the increase in intensity of this same band below 75 K (Figure 4) indicates that the LIESST effect, i.e., LS to light-induced HS state, is occurring at the surface of the sample.

Following this finding, the photomagnetic properties of the **1·MeOH** compound were investigated on a bulk sample using SQUID magnetometry. The drastic increase of the magnetic signal recorded under light irradiation at 10 K confirms the occurrence of LS → HS photoconversion (Figure 5). The limit in $\chi_M T$ reached at photosaturation, after typically 1−2 h of irradiation, was 2.9 cm^3 mol^{-1} K. This value increased slightly, up to 3.3 cm^3 mol^{-1} K at 30 K when the irradiation was ceased and the *T*(LIESST) measurement performed, a feature we attribute to the zero field splitting of the iron(II) center.[18,19] However, comparison of the $\chi_M T$ value recorded at room temperature, which were as expected for a purely HS state, and the $\chi_M T$ value recorded with photoexcitation resulted in nearly 100% photoconversion.

There are two observed minima in the $\delta\chi_M T/\delta T$ vs *T* curve (Figure 5 inset), which defines the limiting temperature *T*(LIESST)[20] above which the light-induced HS information is erased in a SQUID cavity, at 49 (1) and 70 K (2). In comparing the shapes of the $\delta\chi_M T/\delta T$ vs *T* minima, we note that ^2T(LIESST) at 70 K has a sharp minimum, indicative of strong cooperativity.[12] In contrast, ^1T(LIESST) at 49 K is broader. This novel behavior is perhaps not so surprising, as the photomagnetic properties are expected to mirror the thermal SCO process in agreement with the inverse energy gap law defined by Hauser[21] and the empirical relation $T(\text{LIESST}) = T_0 - 0.3T_{1/2}$.[12,19] It is therefore reasonable to connect the interactions that contribute to gradual thermal spin transition at $^1T_{1/2}$ (=197 K) with the light-induced ^1T(LIESST) value (=49 K) and the interactions that contribute to the sharp thermal spin transition at $^2T_{1/2}$ (=98/91 K) with ^2T(LIESST) (=70 K).

Structural Analysis. Single-crystal diffraction data and parameters for the material **1·MeOH** at four temperatures, 25 slow-cooled (25s), 25 quench-cooled (25q), 123, and 293 K, and **2·EtOH** at 123 K, are summarized in Table 1. Selected bond lengths, angles, and additional structural parameters discussed in the text are summarized in Table 2.

1·MeOH. The general structure and the inner coordination numbering scheme of **1·MeOH** are shown in Figure 6. The material consists of a mononuclear iron(II) center with two meridionally coordinated picpzpz ligands, two BF_4^- anions, and one solvent methanol molecule. At all temperatures there is one crystallographically distinct iron(II) center. The bond lengths and angles around the Fe−N_6 core at the different temperatures are listed in Table 2. The average Fe−N bond length at 25 K in the slow-cooled state (25s) is 1.983(3) Å, typical of LS iron(II).[22] For the quench-cooled state at 25 K (25q) and the intermediate plateau at 123 K, these values are 2.068(3) and 2.065(3) Å, respectively, consistent with a random distribution of HS/LS iron(II) sites.[22] The average Fe−N bond length at 293 K is 2.165(4) Å, typical of iron(II) in the fully HS state. Thus, an average change in Fe−N distance of 0.182 Å occurs during the transition LS to HS, consistent with that expected for a full SCO.[22]

(18) Létard, J.-F.; Chastanet, G.; Nguyen, O.; Marcén, S.; Marchivie, M.; Guionneau, P.; Chasseau D.; Gütlich, P. *Monatsh. Chem.* **2003**, *134*, 165.

(19) Létard, J.-F.; Guionneau, P.; Nguyen, O.; Costa, J. S.; Marcén, S.; Chastanet, G.; Marchivie, M.; Goux-Capes, L. *Chem. Eur. J.* **2005**, *11*, 4582.

(20) Létard, J.-F.; Guionneau, P.; Rabardel, L.; Howard, J. A. K.; Goeta, A. E.; Chasseau D.; Kahn, O. *Inorg. Chem.* **1998**, *37*, 4432.

(21) (a) Hauser A. *Coord. Chem. Rev.* **1991**, *111*, 275. (b) Hauser A. *Top. Curr. Chem.* **2004**, *234*, 155.

(22) Real, J. A. In *Transition Metals in Supramolecular Chemistry*; Sauvage, J. P., Ed.; J. Wiley and Sons, Ltd.: New York, 1999; p 53.

Table 2. Selected Fe−N Bond Lengths, Angles, and Parameters for **1·MeOH** at 25(s) K, 25(q) K, 123 K, and 293 K and **2·EtOH** at 123 K[a]

	1·MeOH				**2·EtOH**	
Fe− N Bonds(Å)	25s	25q	123	293	Fe−N Bonds (Å)	123
Fe(1)−N(1)	1.999(3)	2.109(3)	2.107(2)	2.230(3)	Fe(1)−N(1)	2.027(3)
Fe(1)−N(3)	1.929(3)	2.005(3)	1.999(2)	2.082(4)	Fe(1)−N(3)	1.914(3)
Fe(1)−N(5)	2.044(3)	2.104(3)	2.100(3)	2.195(4)	Fe(1)−N(5)	2.013(3)
Fe(1)−N(6)	2.034(3)	2.127(3)	2.125(2)	2.259(4)	Fe(1)−N(6)	1.994(3)
Fe(1)−N(8)	1.920(3)	1.996(3)	1.989(2)	2.072(3)	Fe(1)−N(8)	1.909(3)
Fe(1)−N(10)	2.010(3)	2.067(3)	2.067(3)	2.153(4)	Fe(1)−N(10)	2.042(3)
$<d_{Fe-N}>$ Å	1.989(3)	2.068(3)	2.065(3)	2.165(4)	$<d_{Fe-N}>$ Å	1.983(3)
cis-N−Fe−N (°)					*cis*-N−Fe−N (°)	
N(1)−Fe(1)−N(3)	78.83(13)	76.93(10)	76.82(10)	74.45(14)	N(1)−Fe(1)−N(3)	78.91(14)
N(1)−Fe(1)−N(6)	88.90(12)	87.61(9)	87.51(8)	86.02(13)	N(1)−Fe(1)−N(6)	87.51(12)
N(1)−Fe(1)−N(8)	91.48(12)	91.09(9)	91.36(9)	91.94(13)	N(1)−Fe(1)−N(8)	91.48(14)
N(1)−Fe(1)−N(10)	91.02(12)	91.46(10)	91.57(9)	92.72(13)	N(1)−Fe(1)−N(10)	92.21(13)
N(3)−Fe(1)−N(5)	90.30(13)	87.70(11)	87.57(10)	84.84(14)	N(3)−Fe(1)−N(5)	90.45(14)
N(3)−Fe(1)−N(6)	90.00(12)	90.64(9)	90.71(9)	90.59(14)	N(3)−Fe(1)−N(6)	91.92(14)
N(3)−Fe(1)−N(10)	100.63(12)	104.22(10)	104.20(10)	109.12(15)	N(3)−Fe(1)−N(10)	98.40(14)
N(5)−Fe(1)−N(6)	92.00(11)	92.21(9)	92.24(9)	92.62(13)	N(5)−Fe(1)−N(6)	89.51(13)
N(5)−Fe(1)−N(8)	99.36(12)	103.85(10)	103.78(10)	107.63(13)	N(5)−Fe(1)−N(8)	98.58(14)
N(5)−Fe(1)−N(10)	90.12(12)	92.74(10)	92.77(9)	95.70(13)	N(5)−Fe(1)−N(10)	92.67(13)
N(8)−Fe(1)−N(6)	79.06(12)	76.77(9)	76.61(9)	73.95(14)	N(8)−Fe(1)−N(6)	79.85(14)
N(8)−Fe(1)−N(10)	90.10(12)	87.79(10)	87.90(10)	85.34(14)	N(8)−Fe(1)−N(10)	89.60(13)
trans-N−Fe−N (°)					*trans*-N−Fe−N (°)	
N(1)−Fe(1)−N(5)	169.10(12)	164.62(9)	164.38(10)	159.21(13)	N(1)−Fe(1)−N(5)	168.85(14)
N(3)−Fe(1)−N(8)	165.58(11)	163.07(8)	163.13(9)	160.25(13)	N(3)−Fe(1)−N(8)	167.67(13)
N(6)−Fe(1)−N(10)	169.16(12)	164.51(9)	164.45(9)	159.18(14)	N(6)−Fe(1)−N(10)	169.43(14)
Σ (°)	48.22(12)	69.41(9)	70.22(9)	95.72(14)	Σ (°)	50.33(15)
Φ (°)	3.98	4.99	5.03	6.40	Φ (°)	3.64

[a] See Figure 3 for atom labeling scheme. N(1)−N(3)−N(5) and N(6)−N(8)−N(10) are meridional positions of the picpzpz ligands (see Figure 6). The octahedral distortion parameter, Σ, is given by Σ = summation of the 12 $|90 - \varphi|$ angles where φ are the N−Fe−N cis angles.[8,24] The average trigonal distortion angle, Φ, was calculated from the 24 trigonal angles in the manner recently reported by Real et al.[22,23] Thus, Φ, can be defined as $\Phi = \sum_1^{24} (|60 - \theta|)/24$, where θ represents the trigonal angles defined by two opposed faces of the octahedron, thus giving a total of 24 trigonal angles.

The trans and cis N−Fe−N angles for **1·MeOH** at the different temperatures are listed in Table 2. As the ligand picpzpz is a nonplanar, meridional ligand with sp^3 carbon atoms, distortions within the $Fe-N_6$ octahedron are created such that departures from the expected 90° (cis) and 180° (trans) angles for a regular octahedral system are anticipated.[23] The biggest distortions in the cis angles are those in N(1)−Fe−N(3), N(3)−Fe−N(10), N(5)−Fe−N(8), and N(8)−Fe−N(6) (Table 2). With decreasing temperature, the complex tends toward a more regular geometry, with the cis N−Fe−N angles that exceed 100° becoming smaller and those less than 80° becoming larger. The three trans N−Fe−N angles, which are all ca. 160° at 293 K, increase by 5−10° with cooling to 25 K, in line with the corresponding contraction of the Fe−N distances. Another measure of distortion, the average trigonal distortion angle, Φ, is tabulated in Table 2 at the various temperatures (see Table 2 footnote for calculations). The change in Φ, from 3.98° (LS) to 6.40° (HS), is consistent with the different spin states observed at the different temperatures, since the LS complexes generally have more regular symmetry than their HS counterparts.[22,23] The other commonly reported distortion parameter, Σ, which is the sum of the deviations of the 12 N−Fe−N cis angles from 90°, was also calculated at the different temperatures.[8] Here, Σ changes from 48.44(12)° for the LS state (25s), which is comparable to the ca. 47° reported for related LS compounds,[24] to 95.72(14)° for the HS state (293), slightly higher than the typical value of 85°.[24]

Further structural analysis at each temperature for **1·MeOH** reveals not only that the inner coordination environment of the iron(II) center varies over the spin transition but that subtle changes occur in the orientations and interactions of the methanol solvent molecules and the BF_4^- anions. Figure 7 shows the anion and solvent order/disorder and interactions at each of the different temperatures. There are a number of different hydrogen-bonding interactions between the methanol and BF_4^- anion that vary with temperature and spin state; these appear to play an important role in the observed two-step crossover with an abrupt transition at low temperature and a gradual transition at high temperature.

For the complex slow-cooled to 25 K (25s), all of the solvent methanol and BF_4^- anions were ordered and only one distinct hydrogen-bonding interaction was evident (O30···F8 = 2.837(3) Å, Figure 6a). Notably, the other BF_4^- anion is not involved in any short interactions. In contrast, for the complex quench-cooled to 25 K (25q), each of the BF_4^- anions are now involved in hydrogen-bonding interactions due the solvent methanol being frozen in a disordered state (O30A···F8 = 2.795(4) and O30B···F3 = 2.903(6) Å, Figure 6b). At 123 K, the interactions are largely the same as for the quench-cooled material, as is its magnetic state, where the solvent methanol is disordered and interacting with both

(23) Ortega-Villar, N.; Thompson, A. L.; Muñoz, M. C.; Ugalde-Saldívar, V. M.; Goeta, A. E.; Moreno-Esparza, R.; Real, J. A. *Chem. Eur. J.* 2**005**, *11*, 5721.

(24) Guionneau, P.; Marchivie, M.; Bravic, G.; Létard, J. -F.; Chasseau, D. *J. Mater. Chem.* **2002**, *12*, 2546.

BF_4^- anions (O30A···F8 = 2.825(6) and O30B···F3 = 2.912(6) Å, Figure 6c). In addition, at 123 K a further interaction exists with one of these BF_4^- anions which is disordered (O30B···F4A = 3.315(8) and O30···F4B = 3.005(7) Å, Figure 6c), resulting in a total of four possible interactions at this temperature. With heating to 293 K, similar disorder was found, as was the case for the 123 K refinement, where the solvent methanol and one BF_4^- anion is disordered. Again, both BF_4^- anions are involved in hydrogen-bonding interactions; however, one orientation of the disordered BF_4^- anion is no longer involved, resulting in only three possible interactions (O30A···F8 = 3.018(18), O30B···F3 = 3.108(14), and O30B···F4A = 2.809(19) Å, Figure 6d).

A series of inter-mononuclear interactions exist between the unbound nitrogen atoms of the pyrazine rings and the π ring of a pyrazine in the neighboring molecule (Figure 8). These occur in the *ab* plane, forming sheets of the iron(II) complexes, and separations are typically N(7)···centroid (123 K) = 3.085 Å; N(2)···centroid (123 K) = 3.262 Å (see Table S1 for values over all temperatures). The separations vary with temperature and with slow cooling vs rapid cooling (Table S2). Such interactions in the *ab* plane might influence the changes in unit cell axes lengths shown in Figure 9. When the solvent methanol was removed from **1·MeOH** with heating, the crystallinity was lost and no further structural data could be obtained for comparison.

Variable-Temperature Unit Cell Evolution for 1·MeOH. A less widely used, but highly illuminating, structural approach in monitoring SCO transitions is the measurement of unit cell over the transition temperature range. Figure 9 shows the unit cell parameter evolution versus temperature for **1·MeOH**. First, the material was quench-cooled to 25 K (25q). With heating, the unit cell volume and parameters were found to remain approximately constant between 25 and 60 K. Above 60 K, a rapid decrease in the unit cell volume was observed as the material relaxed from the metastable half-spin state to the LS state. The *b* and *c* axes followed the same downward trend as the unit cell volume, while the *a* axis showed a rapid increase over the same temperature. As described above, there exists in the *ab* plane a network of intermolecular interactions between adjacent mononuclear molecules, while no such interactions exist along the *c* axis (Figure 8). As a consequence of the spin transition, these interactions change in length and mirror the observed variation in unit cell parameters (Table S3). Those interactions located largely along the *a* axis, namely N(7)···C(H)π (Figure 8), are similar in length in the HS and LS states, ca. 3.122(3) Å for 25s, and decrease in length in the intermediate states, ca. 3.052(5) Å for 25q. Those interactions located largely along the *b* axis, namely N(2)···C(H)π (Figure 8), decrease from the LS to HS states, ca. 3.583(3) Å for 25s to 3.240(10) Å for 293 K.

With further heating from 60 to 125 K, the unit cell volume increased gradually to 80 K with thermal expansion, followed by a rapid increase between 80 and 95 K as the abrupt low-temperature spin transition occurred. The crystal was then cooled slowly to 25 K (25s) to achieve the full LS state via an abrupt transition in the range 80−75 K. Here, most impressively, the unit cell volume evolution clearly reflects the hysteresis observed by magnetic susceptibility. The unit cell volume now attained a minimum of 1466(2) $Å^3$, compared to 1485(3) $Å^3$ for the quench-cooled state. Above 95 K the unit cell volume then increased gradually in agreement with the second and more gradual step of the spin transition (Figure 9). The *b* and *c* axes mirror the behavior of the unit cell volume over all temperatures, with the more significant alterations along the *c* axis. The *a* axis, as discussed above, shows the opposite behavior in the region of the hysteresis but for the second more gradual crossover above 100 K follows that of the unit cell volume. The β angle of the monoclinic cell shows quite dramatic variation over the hysteretic transition but is essentially unchanged through the gradual transition.

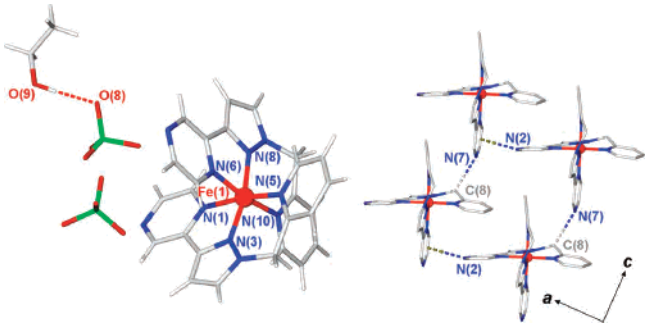

Figure 10. Stick representation of the structure, atomic labeling scheme and hydrogen bonding interaction (···) for **2·EtOH** (left). Intermolecular contacts in the *ac* plane for **2·EtOH** of the type N(lone pair)·π of the neighboring pyrazine π-system, and N(lone pair)·CH_2 (right).

2·EtOH. The structure of the iron(II) complex and associated anion and solvate molecule, for **2·EtOH**, is shown in Figure 10. Crystal data for measurements made at 123 K are given in Table 1, and important iron(II)−ligand bond distances and angles are given in Table 2. The average Fe−N distance of 1.983(3) Å at 123 K is indicative of LS iron(II), consistent with the magnetic study. Calculation of the octahedral distortion parameter, Σ = 50.33(15)°, and the trigonal distortion parameter, Φ = 3.64°, show that the distortion of the iron(II) coordination geometry is similar to that for the LS form of **1·MeOH**, as given in Table 2. A hydrogen-bonding interaction occurs, in a related way to that in **1·MeOH**, between the ethanol and one of the ClO_4^- anions (O(9)···O(8) = 2.875(5) Å, Figure 10).

The mononuclear units lie in sheets in the *ac* plane, and as observed for **1·MeOH**, intermolecular interactions occur between adjacent molecules; N(pyrazine)···aromatic CH (N(2)···CH = 3.225 Å) along the *a* axis and N(pyrazine)···CH_2 (N(7)···CH_2 = 3.236 Å) along the *c* axis (Figure 10). In contrast to **1·MeOH**, the magnetic data show that no abrupt transition occurs at low temperatures. While the change in anion and solvent from **1·MeOH** to **2·EtOH** give similar hydrogen-bonding interactions, they clearly differ sufficiently different in detail to lead to the marked differences in crossover properties observed.

Discussion

We focus first on the key compound, **1·MeOH**, and show that a cohesive picture of its spin transition behavior has emerged from the structural, magnetic, and photomagnetic results. Beginning with the structural data, the changes in the iron−ligand coordination environment that occur between 300 and 25 K, in both slow-cooled and quench-cooled modes, expressed in terms of the various octahedral distortion parameters, are consistent with the transition from a HS state at 293 K to a LS state at 25 K. Average geometries, applicable to the presence of both spin states, are present at 123 K, a temperature falling in the intermediate, plateau region noted in both the magnetic susceptibility and unit cell parameter data.

Equally relevant are the changes noted in the orientation and interactions of, and between, the non-coordinated methanol and BF_4^- anions. Thus, structural analysis of **1·MeOH** at 25 K, after both slow-cooling and quench-cooling, and at 123 and 293 K, reveal important variations in the hydrogen-bonding interactions between the solvent methanol and anions. With slow-cooling to the LS state, only one hydrogen-bonding interaction is observed, whereas with quench-cooling, the methanol is frozen into a disordered state resulting in a broader array of hydrogen-bonding interactions. We attribute both this HS trapping and the observed thermal hysteresis around 90 K to this order/disorder of the solvent molecules, with the memory effect being related to the activation energy barrier for its reorientation. With further heating to the HS state, both the methanol and anion become disordered, and while there are still hydrogen-bonding interactions present between the solvent and anion, the degree of disorder and longer lengths of these interactions evidently confer a lower degree of cooperativity, hence the more gradual step at higher temperatures. A subtle local inhomogeneity of iron(II) environments resulting from the anion and solvent disorder may also serve to broaden the high-temperature transition. Such a detailed result provides a useful insight into the structural factors that may influence cooperativity in other SCO systems. Indeed, we note that 'supramolecular' effects of the kinds just discussed are known to play important, though often unpredictable, roles in SCO materials and some recent examples include tripodal hexadentate compounds of Fe(II),[25,26] a two-step iron(II) compound displaying hydrogen-bonding to ClO_4^-,[27] and a family of bis-meridional tridentate chelates displaying all such features, as well as crystal packing effects involving long alkyl chains attached to the ligand periphery.[4] These studies did not explore the intermolecular structural changes in the level of detail provided here.

A feature of the present structural study on **1·MeOH** has been the use of detailed unit cell parameter variations and comparisons to the magnetic data, particularly the observation of thermal hysteresis. Other groups have recently made related studies. For example, Halcrow and Howard and coworkers[6] reported cell parameter variations in a meridionally chelated $[Fe(L)_2](BF_4)_2$ system (L = 2,6-di(3-methylpyrazol-1-yl)-pyrazine) but with no thermal hysteresis noted in that case. An unusual two-stage SCO was noted for the latter complex, being sharp at ca. 200 K, then gradual below this. Crystallographic order−disorder in the BF_4^- anion was postulated to control the spin transition.[6] In other relevant work, Bürgi et al. noted two order−disorder transitions, with long-range structural order occurring between two distinct Fe sites, to explain the presence of an intermediate crystalline phase change, at $T_{1/2}$, during variable-temperature structural studies on the well-known two-step SCO material $[Fe(2\text{-pic})_3]Cl_2$·EtOH (pic = picolylamine).[28] The unit cell constants in the range 108−290 K were followed in great detail by synchrotron X-ray measurements but no hysteresis was apparent.[28] Real et al. reanalysed a well-known mononuclear SCO material, $[Fe(bt)_2(NCS)_2]$ (bt = 2,2′-bithiazoline), which forms in two polymorphic phases, one of which shows an abrupt spin transition with hysteresis ($T_{1/2}^{\uparrow}$ = 187 K and $T_{1/2}^{\downarrow}$ = 176 K);[9] characterization of the unit cell parameters in the range of the hysteresis loop, 150−200 K, using a limited number of temperature points, showed this hysteresis.[9] Furthermore, the mixed-valence Prussian blue analogue, $CsFe^{II}[Cr^{III}(CN)_6]$ showed a SCO with a 37 K hysteresis loop centered around ca. 225 K and has been studied in detail by high-resolution synchrotron powder X-ray diffraction to reveal hysteresis in the unit cell constants.[10]

The magnetic results for **1·MeOH** show some very interesting features that correlate well with the structural data. Both quench cooling and irradiation of this complex leads to trapping of metastable HS sites at low temperature. Close comparison of the data, however, reveals a significant difference in the nature of these metastable states: for the quench-cooled sample, only one T(TIESST) value was observed at 70 K (Figures 2), while for the light-induced phenomenon, two minima were seen at ^1T(LIESST) = 49 K and ^2T(LIESST) = 70 K (Figure 5). The structural origins of this novel difference, as well as the thermal hysteresis observed in the abrupt low-temperature step and the contrasting gradual step noted at higher temperatures, are all well explained by the temperature-dependent solvent−anion structural interactions discussed above. We note that observation of two minima in a T(LIESST) experiment has been reported previously for the SCO mononuclear compound $[Fe(DPEA)(bim)](ClO_4)_2$·$0.5H_2O$ (DPEA = 2-aminoethyl-bis-(2-pyridylmethyl)amine and bim = 2,2-bisimidazole) and attributed to the existence of two different lattice sites for the iron(II) atoms.[27]

In the broader context of comparing the present T(LIESST) values for **1·MeOH** with those previously reported in a T(LIESST)-$T_{1/2}$ database reported by Létard[12,19] (Figure S4),

(25) Sunatsuki, Y.; Ohta, H.; Kojima, M.; Ikuta, Y.; Goto, Y.; Matsumoto, N.; Iijima, S.; Akashi, H.; Kaizaki, S.; Dahan, F.; Tuchagues, J. -P. *Inorg. Chem.* **2004**, *43*, 4154.

(26) Ikuta, Y.; Ooidemizu, M.; Yamahata, Y.; Yamada, M.; Osa, S.; Y.; Matsumoto, N.; Iijima, S.; Sunatsuki, Y.; Kojima, M.; Dahan, F.; Tuchagues, J.-P. *Inorg. Chem.* **2003**, *42*, 7001.

(27) Matouzenko, G.S.; Létard, J. -F.; Lecocq, S. Bousseksou, A.; Capes, L.; Salmon, L.; Perrin, M.; Kahn, O.; Collet, A. *Eur. J. Inorg. Chem.* **2001**, 2935.

(28) Chernyshov, D.; Hostettler, M.; Törnoos, K. W.; Bürgi, H. B. *Angew. Chem., Int. Ed.* **2003**, *42*, 3825.

and trying to determine the empirical parameter T_0 that corresponds to the y intercept defined by the data,[12,19] it is interesting to find that the two T(LIESST) values of **1·MeOH** can be placed on the $T_0 = 100$ K line. To now, the detailed physical origin of T_0 is uncertain but appears to depend primarily on the geometry and conformational rigidity of the ligand donors about the metal ion.[12,19] Factors outside the inner metal coordination sphere, such as intermolecular cooperativity, crystal packing, and the nature of any anions and solvent in the material, typically result in only minor perturbations to T_0 for a given set of metal complexes.[12] To date, four series of compounds that show parallel T_0 lines have been demonstrated, with values of 100 K for Fe(II) complexes of monodentate ligands,[29]120 K for system with bidentate ligands,[29] 150 K for systems involving meridional tridentate ligands,[6,30,31] and 200 K for three-dimensional network solids.[32] In addition, we have noticed that for SCO complexes with tridentate ligands possessing some degree of freedom carried by unsaturated carbon atom between the aromatic rings the T(LIESST) values follow the $T_0 = 100$ K line.[33,34] This emphasizes the concept that vibrational aspects and hardness of the inner coordination sphere are the key factors for stabilizing the metastability of the light-induced HS state.[12,19] Thus, the observations found here for the **1·MeOH** complex, where the tridentate picpzpz ligand possesses a flexible unsaturated carbon atom connecting the aromatic pyrazole and pyrazine rings, show that it is a new example of a non-optimized ligand system in regard to the stabilization of the light-induced HS state. The previous conclusions made with respect to the now extensive T(LIESST)-$T_{1/2}$ database, nevertheless, remain valid.

Turning briefly to the desolvated material, **1**, it is noteworthy that the magnetic data do not show the sharp step in the spin transition at 90 K nor do they display any thermal hysteresis (Figure 2). Therefore, it again seems likely that the sharp step, with its hysteresis, can be attributed to the strong solvent−anion hydrogen-bonding interactions described above.

The other structurally characterized member of the present family, **2·EtOH**, containing the same picpzpz ligand, but with different anion (ClO_4^- vs BF_4^-) and solvent (EtOH vs MeOH) compared to **1·MeOH**, shows related structural nuances. However, in contrast to **1·MeOH**, the magnetic data show that no abrupt transition occurs at low temperatures. While the change in anion and solvent from **1·MeOH** to **2·EtOH** give similar hydrogen-bonding interactions, they clearly differ sufficiently in detail to lead to the marked differences in crossover properties observed. The magnetic data for the picpzpz compounds **1·EtOH** and **2·MeOH** and for the related picpypz compound **3·MeOH** all show gradual spin transitions (Figure 2), the $\chi_M T$ values not reaching the HS values below 350 K. In the absence of structural data, we assume that, as in **2·EtOH**, there are no specific and strong anion−solvent interactions of the type observed in **1·MeOH**, capable of producing sharp spin transitions and/or thermal hysteresis.

Conclusions

A family of iron(II) SCO monomers containing the bis-meridional ligands picpzpz and picpypz has been synthesized. Of these, the complex **1·MeOH** is particularly noteworthy in displaying an interesting two-step spin transition that comprises a gradual high-temperature step and an abrupt low-temperature step with a hysteresis gap of 7 K, ${}^1T_{1/2} = 197$ K and ${}^2T_{1/2} = 91/98$ K. Thermal trapping of the HS state is observed with quench-cooling. The abrupt hysteretic spin transition is lost following removal of the solvent methanol molecule to form **1**, which undergoes a gradual incomplete SCO with $T_{1/2} = 150$ K. The loss of the low-temperature step is consistent with the observation that reorientation of the methanol molecule plays an intrinsic role in the low-temperature crossover step in **1·MeOH**. The observed decrease in the temperature of the high-temperature gradual step, by ca. 50 K, is attributed to crystal packing effects.

Three analogues of **1·MeOH** in which the solvent and anion were varied systematically, **1·EtOH**, **2·MeOH**, and **2·EtOH**, and the related complex **3·MeOH**, in which the pyrazine ring of picpzpz is replaced with a pyridine ring, all show gradual one-step spin transitions with $T_{1/2}$ values in the range 210−250 K; these serve to further highlight the extreme sensitivity of the SCO phenomenon to subtle structural modification.

In addition to its novel two-step behavior, **1·MeOH** is one of very few compounds known to display a two-step LIESST relaxation process with two T(LIESST) temperatures. Interestingly, one of these steps is abrupt and one gradual, mirroring the two thermal transitions. Comparison of the T(LIESST) vs $T_{1/2}$ relation $T(\text{LIESST}) = T_0 - 0.3T_{1/2}$,[12,19] for **1·MeOH**, to those observed for a large database of iron(II) SCO compounds, has yielded a T_0 value that indicates the picpzpz ligand is non-optimized in stabilizing the metastable HS state under green light irradiation at low temperatures.

Variable-temperature unit cell measurements on **1·MeOH** display both the gradual and abrupt transitions, the quench-cooled state and the observation of thermal hysteresis. To our knowledge these results are the most detailed reported thus far for SCO systems, with a remarkable agreement achieved with the magnetic data. We believe this largely unexploited technique will be invaluable for future SCO materials characterization, in particular, toward elucidating definitively the relative roles of inter- and intramolecular interactions over the entirety of the spin transition temperature range.

(29) Létard, J.-F.; Capes, L.; Chastanet, G.; Moliner, N.; Létard, S.; Real J. A.; Kahn, O. *Chem. Phys. Lett*. **1999**, *313*, 115.
(30) Marcén, S.; Lecren, L.; Capes, L.; Goodwin, H. A.; Létard, J.-F. *Chem. Phys. Lett*. **2002**, *358*, 87.
(31) Carbonera, C.; Costa, J. S.; Money, V. A.; Elhaïk, J.; Howard, J. A. K.; Halcrow M. A.; Létard, J.-F. *Dalton Trans.* **2006**, 3058.
(32) Shimamoto, N.; Ohkoshi, S.-S.; Sato, O.; Hashimoto, K. *Inorg. Chem.* **2002**, *41*, 678.
(33) Bonhommeau, S.; Brefuel, N.; Pálfi, V. K.; V.; Malnár, G.; Zwick, A.; Salmon, L.; Tuchagues, J.-P.; Costa, J. S.; Létard, J.-F.; Paulsen, H.; Bousseksou, A. *Phys. Chem. Chem. Phys.* **2005**, *7*, 2909.
(34) Enachescu, C.; Linares, J.; Varret, F.; Boukheddaden, K.; Codjovi, E.; Salunke, S. G.; Mukherjee, R. *Inorg. Chem*. **2004**, *43*, 4880.

Acknowledgment. The Australian Research Council, ARC, is thanked for providing a Discovery Grant to support this work. Financial support for the photomagnetic LIESST work was kindly provided by a French−Australia FAST/DEST grant and this allowed the Australian participants to travel to Bordeaux to carry out measurements.

Supporting Information Available: Single-crystal X-ray diffraction analysis, tables of hydrogen-bonding and intermolecular interactions, and a database of $T_{1/2}$ vs T(LIESST). This material is available free of charge via the Internet at http://pubs.acs.org.

IC7010919